

# Evidence of enhanced two-level system loss suppression in high-Q, thin film aluminum microwave resonators

Carolyn G. Volpert

*Astronomy Department, University of Maryland, College Park, Maryland 20742, USA and  
NASA Goddard Space Flight Center, Goddard, Maryland 20771, USA\**

Emily M. Barrentine, Ari Brown, Jake A. Connors, Thomas Essinger-Hileman,  
Larry A. Hess, Vilem Mikula, Thomas R. Stevenson, and Eric R. Switzer  
*NASA Goddard Space Flight Center, Goddard, Maryland 20771, USA\**

Alberto D. Bolatto

*Astronomy Department, University of Maryland, College Park, Maryland 20742, USA  
(Dated: December 13, 2024)*

As superconducting kinetic inductance detectors (KIDs) continue to grow in popularity for sensitive sub-mm detection and other applications, there is a drive to advance toward lower loss devices. We present measurements of diagnostic thin film aluminum coplanar waveguide (CPW) resonators designed to inform ongoing KID development at NASA Goddard Space Flight Center. The resonators span  $f_0 = 3.5 - 4$  GHz and include both quarter-wave and half-wave resonators with varying coupling capacitor designs. We present measurements of the device film properties and an analysis of the dominant mechanisms of loss in the resonators measured in a dark environment. We demonstrate quality factors of  $Q_i^{-1} \approx 3.64 - 8.57 \times 10^{-8}$ , and observe enhanced suppression of two-level system (TLS) loss in our devices at high internal microwave power levels before the onset of quasiparticle dissipation from microwave heating. We observe deviations from the standard TLS loss model at low powers and temperatures below 60 mK, and use a modified model to describe this behavior.

## I. INTRODUCTION

Superconducting microwave resonators have gained traction in recent years both for applications in optical detection – particularly at far-infrared (FIR) and sub-millimeter (sub-mm) frequencies – and as components in quantum computing circuits. Such resonators are attractive for use in astronomical instruments as kinetic inductance detectors (KIDs) due to their high sensitivity paired with their unique advantage of frequency-domain multiplexing.

At present, one of the largest obstacles facing applied superconducting resonator technology is our ability to mitigate and otherwise predictably model sources of signal loss in a resonator, both through optimizing fabrication processes and establishing dynamic measurement-based models for signal loss. The relative novelty and diversity of applications for these devices drives the field to seek more ideal materials, fabrication processes, designs, and integrations to push devices towards fundamental performance limits. Both KID and quantum computing applications incentivize scaling up resonator array sizes while maintaining high sensitivity, low noise, and array uniformity. This places a special importance upon understanding the loss mechanisms of superconducting microwave resonators, which manifest as decoherence in quantum circuits and as a reduction in optical responsivity and increase in noise in optical detectors.

The optical responsivity of a material is determined by both its internal quality factor  $Q_i$  and by its kinetic inductance fraction  $\alpha$ . Materials with both high quality factors and high kinetic inductance fractions provide greater sensitivity to photons. However contaminants introduced during fabrication processes will often induce loss by introducing parasitic two-level systems (TLS) to materials. This motivates choosing film materials and fabrication techniques that prevent contaminants when possible and selecting for contaminants that generate fewer TLS when necessary. For applications in detection it is also important to consider a material's superconducting energy gap  $\Delta_0$ , as superconducting resonators will not respond to photons with energies  $h\nu < 2\Delta_0$ . This naturally constrains the range of materials suited to KID design to those well-matched to the frequency range of the photons being detected. With these considerations in mind materials such as TiN, NbTiN, Nb, Re, and Al have arisen as popular material candidates for use in fabricating infrared and sub-mm KIDs. In this work we present measurement results for thin film Al on Si coplanar waveguide (CPW) resonators designed for use in far-infrared astronomy, focusing on the intrinsic film properties and sources of loss in the resonators.

\* cvolpert@astro.umd.edu; c.g.volpert@nasa.gov

## II. EXPERIMENTAL SETUP

### A. Device design and fabrication

Our device contains sixteen CPW resonators coupled to a central CPW feedline. The resonators were wet-etched into a 23 nm thick film of Al sputter deposited on Si. The device architecture requires the patterning of only a single layer, and was chosen to simplify fabrication, provide more rapid turnaround of test devices, and to be dynamically applicable to measuring the properties of several superconducting materials. For this reason the device incorporates a variety of coupling capacitors, with finger-capacitor structures that cycle between three lengths (0  $\mu\text{m}$ , 10  $\mu\text{m}$ , and 30  $\mu\text{m}$ ) to provide coverage for a range of internal quality factors. The feedline was designed with an impedance of 50  $\Omega$ . Fifteen resonators are  $\lambda/4$ , and the sixteenth resonator is  $\lambda/2$  and couples to the feedline with a 30  $\mu\text{m}$  finger-capacitor structure. The device has no optical inputs and is packaged in a container designed to be light-tight, so contributions from optical photons are not considered in these results. In this work we focus here on data from a representative  $\lambda/4$  resonator and our  $\lambda/2$  resonator. The devices were fabricated in the Detector Development Lab at NASA Goddard Space Flight Center (GSFC) and all testing was performed at GSFC.

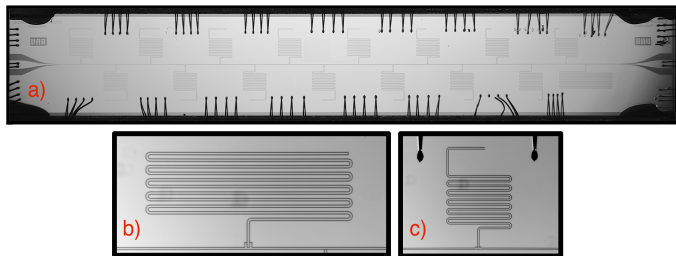


FIG. 1. a) An image of the entire test chip, which includes fifteen quarter-wave resonators and one half-wave resonator coupled to a central feedline. b) The half-wave resonator. c) The quarter-wave resonator.

Steps in the fabrication process were designed to control formation of native oxides. First, we clean the float-zone Si substrate before sputter depositing the Al. We pay special attention to the conditions of the sputtering process to control the quality of the deposited Al. After deposition, we perform an additional in situ clean. Without this additional cleaning step, in some cases we have found residual irregular patches of Al on the silicon after etching. We then adhere a photoresist to the Al with hexamethyldisilazane (HMDS) and wet-etch the microwave circuit. We remove the photoresist layer with a solvent, and remove the the HMDS with  $\text{O}_2$  ashing before finally dicing the wafer.

TABLE I. The following quantities were measured either using the test device, or the Al on Si wafer from which the device was spliced. Dashes denote the  $\lambda/2$  value applies to all resonators.

Parameter	$\lambda/2$	$\lambda/4$
Al film Thickness <sup>a</sup>	23 $\pm$ 1 nm	–
Feedline $T_c$ <sup>a</sup>	1.31 $\pm$ 0.03 K	–
Resistivity <sup>a</sup> , $\rho_n$	5.5 $\times$ 10 <sup>-8</sup> $\Omega$ m	–
Sheet Resistance <sup>a</sup> , $R_s$	0.483 $\Omega$ /sq	–
Resonant Frequency <sup>a</sup> , $f_r$	3.911 GHz	3.655 GHz
Resonator Length <sup>b</sup>	7.283 mm	13.939 mm
CPW Width <sup>b</sup>	10 $\mu\text{m}$	–
CPW Gap <sup>b</sup>	5 $\mu\text{m}$	–
Coupling Structure Length <sup>b</sup> <sup>c</sup>	30 $\mu\text{m}$	10 $\mu\text{m}$
$Q_c(\times 10^5)$ <sup>a</sup>	0.87	2.58
Minimum $Q_i^{-1}(\times 10^{-8})$ <sup>a</sup>	3.64 $\pm$ 0.11 <sup>d</sup>	8.57 $\pm$ 0.17 <sup>e</sup>

<sup>a</sup> Measured

<sup>b</sup> Design

<sup>c</sup> The finger length of the coupling capacitor structures connecting to the feedline.

<sup>d</sup> at 60 mK,  $\bar{n}_{\text{ph}} \approx 4.8 \times 10^7$

<sup>e</sup> at 18 mK,  $\bar{n}_{\text{ph}} \approx 5.6 \times 10^6$

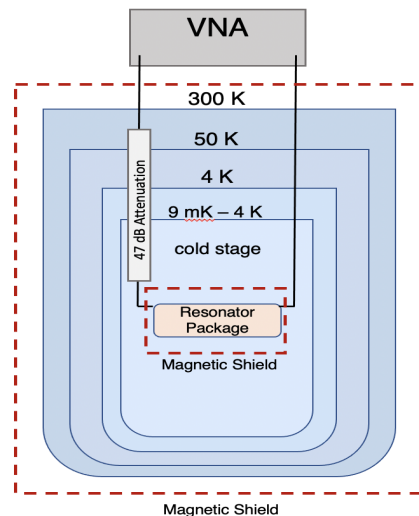


FIG. 2. The cryogenic testbed configuration. The test chip was situated within layers of magnetic shields on a temperature controlled cold stage. Read tone generation and return signal readout was performed using a VNA at room temperature. There was a cumulative 47 dB of attenuation between the read tone output at the VNA and the input to the resonator package on the cold stage.

### B. Measurement setup

To measure our device's microwave properties we mounted it in a 'dark' (un-illuminated and stray-light mitigated) dilution refrigerator beneath two layers of magnetic shielding (Figure 2) on a temperature controlled stage. We took measurements at several temper-

atures ranging from 9 mK (base) to 400 mK. We read out the device using an Agilent Technologies PNA-X vector network analyzer (VNA). The read tone from the VNA was cumulatively attenuated by -47 dB (via microwave cabling, etc.) before reaching the device input on the innermost stage. We used the VNA to measure the forward transmission through the system  $S_{21} = I + iQ$  (where  $I$  is the in-phase component and  $Q$  is the quadrature component in the imaginary plane) as a function of read tone frequency  $f_{\text{read}}$ . We measured  $S_{21}^{\text{meas}}(f_{\text{read}})$  for a variety of device conditions: both varying the power of the input read tone and varying the ambient temperature of the test device,  $T_{\text{bath}}$ . We applied read tone powers  $P_{\text{read}}$  between -137 dBm and -67 dBm (after attenuation) and varied  $T_{\text{bath}}$  between 9 mK and 400 mK.

### III. THEORY

Resonator performance is quantified by the quality factor  $Q_r$ , where  $1/Q_r = 1/Q_i + 1/Q_c$ , where  $Q_i$  the internal quality factor (energy stored in a resonator / loss in a resonator), and  $Q_c$  the coupling quality factor (energy stored in a resonator / loss to coupling).

#### A. Fitting transmission data

To find the resonant frequency  $f_r$  and the  $Q_i$  of a resonator, we fit our  $S_{21}(f_{\text{read}})$  transmission data using a hanger (or notch) type resonator model, which assumes each resonator is a short-circuited transmission line with one end shorted to the ground and the other end side coupled to the central coplanar waveguide (Figure 1). We use the diameter correction method (DCM) version of this model to produce an asymmetrical Lorentzian shape with a dip in magnitude and a shift in phase at the resonant frequency. The ideal DCM hangar model defines the transmission through a resonator as [1]

$$S_{21}(x) = \frac{Q_i^{-1} + 2i(x + \delta x)}{Q_r^{-1} + 2i x} \quad (1)$$

where  $x(f_{\text{read}}) = (f_{\text{read}} - f_r)/f_r$ , and  $\delta x$  accounts for shifts in  $x$  induced by environmental factors (e.g.  $T_{\text{bath}}$ ).

We introduce an additional term to this model to account for effects such as finite length feedlines, internal reflections, and other sources of transmission asymmetry. Our total fit to the data takes the form

$$S_{21}^{\text{meas}} = g(f_{\text{read}}) S_{21}^{\text{res}} e^{i\phi(f_{\text{read}})} \quad (2)$$

$$g(f_{\text{read}}) = g_0 + g_1 x + g_2 x^2$$

$$\phi(f_{\text{read}}) = \phi_0 + \phi_1 x + \phi_2 x^2$$

where  $S_{21}^{\text{meas}}$  is our measurement data,  $g(f_{\text{read}})$  and  $\phi(f_{\text{read}})$  is a frequency-dependent complex gain factor, and  $\phi(f_{\text{read}})$  is

a frequency-dependent complex phase shift factor [1–3]. We modified the Python package `scraps` to fit our large data set with the model we have described [4].

#### B. Loss mechanisms

The inverse internal quality factor  $Q_i^{-1}$  acts as a metric of loss in a resonator, with smaller  $Q_i^{-1}$  values indicating less transmission loss and greater detector sensitivity. When a photon of sufficient energy strikes an Al film it breaks Cooper pairs and generates quasiparticles, changing resonator inductance. However, other extraneous mechanisms can impact the quasiparticle population in a resonator, acting as sources of noise or loss (i.e. power dissipation). Pertinent loss mechanisms include thermal quasiparticle generation, microwave read-tone induced pair breaking, two-level system effects, magnetic vortices, and stray-light induced pair breaking. This work neglects the latter two mechanisms, as we paid special attention to magnetic shielding and stray-light shielding in our experimental design (Figure 2), rendering the loss from these effects negligible in comparison to others. There are no optical inputs to our device, so we can model our total resonator loss as [5]

$$Q_i^{-1} = Q_{i,\text{qp}}^{-1}(T_{\text{bath}}, P_{\text{read}}) + Q_{i,\text{TLS}}^{-1}(T_{\text{bath}}, P_{\text{read}}) + Q_{i,\text{other}}^{-1} \quad (3)$$

where  $Q_{i,\text{qp}}^{-1}$  is a contribution from the excess quasiparticle population in the resonator (from either read-tone power induced pair breaking, or thermal generation recombination),  $Q_{i,\text{TLS}}^{-1}$  is a contribution from two-level system effects, and  $Q_{i,\text{other}}^{-1}$  is a catch all constant term made up of other loss contributions that are temperature and power invariant.

##### 1. Quasiparticle loss

The first loss contribution,  $Q_{i,\text{qp}}^{-1}$ , depends upon the number of quasiparticles present in the resonator  $N_{\text{qp}}$ , and is given by [6]

$$Q_{i,\text{qp}}^{-1} = N_{\text{qp}} \times \frac{2\alpha}{4N_0\Delta V} S_1 \quad (4)$$

where  $\alpha$  is the kinetic inductance fraction,  $N_0 = 1.74 \times 10^{10} \text{ eV}^{-1} \mu\text{m}^{-3}$  is the single-spin density of states at the Fermi level for aluminum (from [7]),  $\Delta = 1.764 T_c k_B$  is the gap energy of the film,  $V$  is the resonator volume, and  $S_1$  is a dimensionless response function defined as [6]

$$S_1 = \frac{2}{\pi} \sqrt{\frac{2\Delta}{\pi k_B T_{\text{bath}}}} \sinh(\xi) K_0(\xi)$$

where  $\xi = \hbar f_r / (2k_B T_{\text{bath}})$ , and  $K_0$  is the 0th order modified Bessel function of the second kind.

The number of quasiparticles in a resonator  $N_{\text{qp}}$  changes both with the bath temperature  $T_{\text{bath}}$  and the read tone power  $P_{\text{read}}$  as [6, 8, 9]

$$N_{\text{qp}} = \sqrt{\frac{V\Gamma_{\text{tot}}}{\mathbf{R}}} \quad (5)$$

$$\mathbf{R} = \frac{(2 \times 1.76)^3}{4N_0\Delta\tau_0 f_{\text{trap}}} \quad (6)$$

where  $\mathbf{R}$  is the effective recombination constant,  $\tau_0 = 438$  ns is the the electron-phonon interaction time for Al [10],  $f_{\text{trap}}$  is a phonon trapping factor (we assume  $f_{\text{trap}} = 2$ ), and  $\Gamma_{\text{tot}}$  is the total quasiparticle generation rate defined as [6]

$$\Gamma_{\text{tot}} = \Gamma_{\text{th}} + \Gamma_{\text{pb}} = (VR \mathbf{n}_{\text{th}}^2) + \left( P_{\text{read}} \frac{\eta_{\text{read}} \chi_{\text{qp}}}{\Delta} \right) \quad (7)$$

$$\mathbf{n}_{\text{th}} = 4N_0\Delta \sqrt{\frac{\pi k_B T_{\text{bath}}}{2\Delta}} e^{-\Delta/k_B T_{\text{bath}}}$$

where  $\eta_{\text{read}}$  is the efficiency for converting read tone power into quasiparticles,  $\chi_{\text{qp}} = Q_{i,\text{qp}}^{-1}/Q_i^{-1}$  is the fraction of internal dissipation due to quasiparticles, and  $\mathbf{n}_{\text{th}}$  is the thermal quasiparticle number density.

Using this model, the loss due to excess quasiparticles has a temperature dependence that looks like  $Q_{i,\text{qp}}^{-1} \propto e^{-1/T_{\text{bath}}} \sinh(1/T_{\text{bath}}) K_0(1/T_{\text{bath}})$  and a read tone power dependence that looks like  $Q_{i,\text{qp}}^{-1} \propto \sqrt{1 + P_{\text{read}}}$ . The quasiparticle loss  $Q_{i,\text{qp}}^{-1}$  depends upon the material film parameters  $\alpha$ ,  $\Delta$ , and  $\eta_{\text{read}}$ .

At high temperatures ( $\geq 200$  mK) and intermediate read tone powers  $Q_{i,\text{qp}}^{-1}$  will strongly dominate the total loss and  $\Gamma_{\text{th}}$  will dominate  $N_{\text{qp}}$ . In this regime we can assume that for a fixed read power  $dQ_{i,\text{tot}}^{-1}/dT_{\text{bath}} \approx dQ_{i,\text{qp}}^{-1}/dT_{\text{bath}} + C$ , where  $C$  is some small constant offset from TLS and  $Q_{i,\text{other}}^{-1}$ , and we can neglect contributions from  $\Gamma_{\text{pb}}$ . We can then fit our  $dQ_i^{-1}/dT_{\text{bath}}$  data in this regime to recover  $\alpha$  and  $T_c$  (via  $\Delta = 1.764 T_c k_B$ ). Using this technique, we find for the half-wave and the quarter-wave respectively  $\alpha = [0.26, 0.26]$ , and  $T_c = [1.37, 1.37]$  K (Tables II, III).

We then used the values we found for  $\alpha$  and  $T_c$  to fit for  $\eta_{\text{read}}$ . At the highest read powers for low temperatures  $Q_{i,\text{qp}}^{-1}$  will dominate the total loss. In this regime we can assume that for a fixed low temperature  $dQ_{i,\text{tot}}^{-1}/dP_{\text{read}} \approx dQ_{i,\text{qp}}^{-1}/dP_{\text{read}} + G$ , where  $G$  is some constant offset from TLS and  $Q_{i,\text{other}}^{-1}$ , and we can use the  $\alpha$  and  $T_c$  values we found to estimate  $\Gamma_{\text{th}}$ . Using this method to fit our  $dQ_{i,\text{tot}}^{-1}/dP_{\text{read}}$  data we find for the half-wave and the quarter-wave respectively  $\eta_{\text{read}} (\times 10^{-3}) = [1.7, 1.8]$  (Tables II, III).

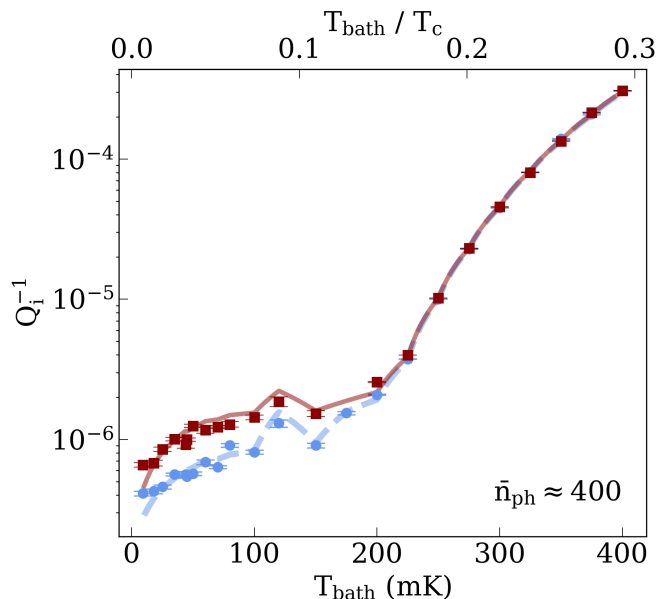


FIG. 3. The loss in a resonator (expressed by  $Q_i^{-1}$ ) as a function of device temperature. The red data and fit are for the  $\lambda/2$  resonator, and the blue data and fit are for the  $\lambda/4$  resonator. The model values between data points are the product of interpolation.

## 2. TLS loss

Although the exact nature of parasitic two-level systems remain unclear, it is thought that TLS arise when defects or impurities in the detector substrate or metal layer cause one or a group of atoms to tunnel between multiple available states with a broad spectrum of transition energies. These fluctuating sites can be excited by absorbing photons from the resonator, and eventually relax and re-emit phonons back into the resonator. This process results in resonator transmission loss and generates phase noise.

TLS loss can originate from several different sources in the device: surface and interface contamination, native surface oxides, and irregularities in the bulk, with surface TLS often dominating smaller devices. The most commonly used Standard Tunneling Model (STM) of two-level systems considers the aggregate loss caused by a population of TLS,  $Q_{i,\text{TLS}}^{-1}$ , to take the form [2]

$$Q_{i,\text{TLS}}^{-1}(n_{\text{ph}}) = F\delta_{\text{TLS}}^0 \tanh(\xi) \left( 1 + \frac{\bar{n}_{\text{ph}}}{n_{\text{ph}}^c} \right)^{-1/2} \quad (8)$$

where  $F$  is a geometric filling factor accounting for the volume the TLS occupy in the resonator,  $\delta_{\text{TLS}}^0$  is the fundamental minimum TLS loss at zero power and temperature,  $\bar{n}_{\text{ph}}$  is the average number of microwave photons in the device, and  $n_{\text{ph}}^c$  is the critical photon number above which the TLS in the device are fully saturated. Since there is no optical source present, the average number of

microwave photons  $\bar{n}_{\text{ph}}$  in the resonator is dictated by the read tone power via the relation [11]

$$\bar{n}_{\text{ph}} = \frac{P_{\text{read}}}{2\pi m} \frac{Q_r^2}{Q_c} \frac{1}{\hbar f_r^2} \quad (9)$$

where  $P_{\text{read}}$  is the read tone power (after attenuation) and  $m = [1/2, 1/4]$  for the  $\lambda/2$  and  $\lambda/4$  resonators respectively is a geometric factor.

While this model is sufficient for many applications, it struggles at very low temperatures and photon occupation numbers, and for TLS with extreme time constants. The standard model assumes a constant  $n_{\text{ph}}^c$ , however it can be shown that  $n_{\text{ph}}^c \propto (T_1 T_2)^{-1}$ , where the average relaxation time  $T_1$  is the timescale associated with going from the TLS excited state to the ground state, and the average dephasing time  $T_2$  is the timescale over which phase information is preserved [12]. These timescales have some temperature dependence, with the relaxation generally following a thermal distribution of  $T_1 \propto \tanh(\xi)$ .

Some works have suggested that contrary to the classical STM assumption, TLS-TLS interactions are not always negligible and state changes in one TLS can dephase neighboring TLS [13]. We can assume that as the temperature decreases and more TLS revert to their ground states, the dephasing time  $T_2$  will inversely increase with fewer neighboring TLS state-changes occurring. Some works have modeled this relation as  $1/T_2 \propto D T_{\text{bath}}^\mu$  where  $D$  is a constant and  $\mu$  is a microscopic parameter relating to the density of states of the TLS population such that generally  $\rho(E) \sim \rho_0(E/E_{\text{max}})^\mu$  [14]. The classical model assumes that TLS-TLS interactions are insignificant and  $\mu = 0$ , however works pursuing TLS-TLS interactions in detail more commonly find  $\mu \approx 1.1 - 2.0$  [13–15]. With this in mind we can now conclude that

$$n_{\text{ph}}^c \propto (T_1 T_2)^{-1} \propto \frac{T_{\text{bath}}^{1+\mu}}{\tanh(\xi)}. \quad (10)$$

Additionally, to account for the fact that tone power modes will saturate the population of TLS systems differently as the device is increasingly occupied by photons, we introduce an empirical fit parameter  $\beta$  to account for read power dependence such that  $\bar{n}_{\text{ph}} \rightarrow \bar{n}_{\text{ph}}^\beta$  [13].

Combining these new assumptions, we can rewrite our model from Eq. 8 as

$$Q_{i,\text{TLS}}^{-1}(n_{\text{ph}}, T_{\text{bath}}) = F\delta_{\text{TLS}}^0 \tanh(\xi) \left(1 + \frac{\tanh(\xi) \bar{n}_{\text{ph}}^\beta}{DT_{\text{bath}}^\mu}\right)^{-1/2} \quad (11) \quad \delta f_{\text{th}} = \frac{f_r(T_{\text{bath}}) - f_r(0)}{f_r(0)} \quad (13)$$

$$= -3.6 \frac{\alpha\pi}{4} \sqrt{\frac{\pi k_B T_{\text{bath}}}{2\Delta_0}} e^{-\Delta_0/k_B T_{\text{bath}}}.$$

To recover  $F\delta_{\text{TLS}}^0$ ,  $\beta$ ,  $D$ , and  $\mu$  for our resonators we first performed fits to our  $dQ_{i,\text{tot}}^{-1}/dT_{\text{bath}}$  data (Figure 4) at the lowest  $P_{\text{read}}$  (where TLS effects are most dominant) using equations 3, 4, and 11 along with our

$\alpha$  and  $T_c$  results from quasiparticle loss fitting, while leaving  $\eta_{\text{read}}$  and  $Q_{i,\text{other}}^{-1}$  as fit parameters. Using this method we found for the half-wave and the quarter-wave respectively  $F\delta_{\text{TLS}}^0 (\times 10^{-6}) = [3.87, 3.47]$ ,  $D = [386, 492]$ , and  $\mu = [1.32, 1.23]$  (Tables II, III).

We used these initial fit results to constrain  $D$  and  $\mu$  (the variables dominating temperature dependent behavior), before then performing fits to our  $dQ_{i,\text{tot}}^{-1}/dP_{\text{read}}$  data (Figure 5) to find universal parameters across sixteen temperatures between 9 mK and 400 mK. We recover  $F\delta_{\text{TLS}}^0$  and  $\beta$  (the variables dominating power-dependent behavior) while leaving  $\eta_{\text{read}}$  as a fit parameter. Using this method we found for the half-wave and the quarter-wave respectively  $F\delta_{\text{TLS}}^0 (\times 10^{-6}) = [3.85, 3.29]$  and  $\beta = [0.76, 0.78]$  (Tables II, III).

### 3. Other loss

The last source of loss we model  $Q_{i,\text{other}}^{-1}$  is a constant, and is the sum of all non temperature or power dependent sources of loss (such as trapped magnetic vortices). From our fitting we found for the half-wave and the quarter-wave respectively  $Q_{i,\text{other}}^{-1} (\times 10^{-8}) = [3.83, 7.23]$  (Tables II, III).

### C. Frequency shifts

We independently crosscheck some of our material parameter fit values by examining the temperature-dependent shift in resonance frequency. We can express this shift as  $f_r$  [5, 16]

$$\delta f_{\text{tot}}(T_{\text{bath}}) = \delta f_{\text{th}}(T_{\text{bath}}) + \delta f_{\text{TLS}}(T_{\text{bath}}) \quad (12)$$

where  $\delta f_{\text{tot}} = f_r(T_{\text{bath}}) - f_r(0) / f_r(0)$  is the total relative shift in resonant frequency at a given temperature,  $\delta f_{\text{th}}$  is the contribution from thermal effects, and  $\delta f_{\text{TLS}}$  is the contribution from TLS effects.

When the ambient temperature of the test device reaches high enough temperatures to begin to produce phonons capable of inducing pair breaking, the quasiparticle population in the resonators changes, resulting in a shift in their resonant frequencies. This thermal phonon-dependent change in resonant frequency,  $\delta f_{\text{th}}$ , can be modeled as [5, 16]

TLS induce a change in  $f_r$  by introducing excess quasiparticles upon de-excitation, and by causing small shifts in the real part of the dielectric constant from associated

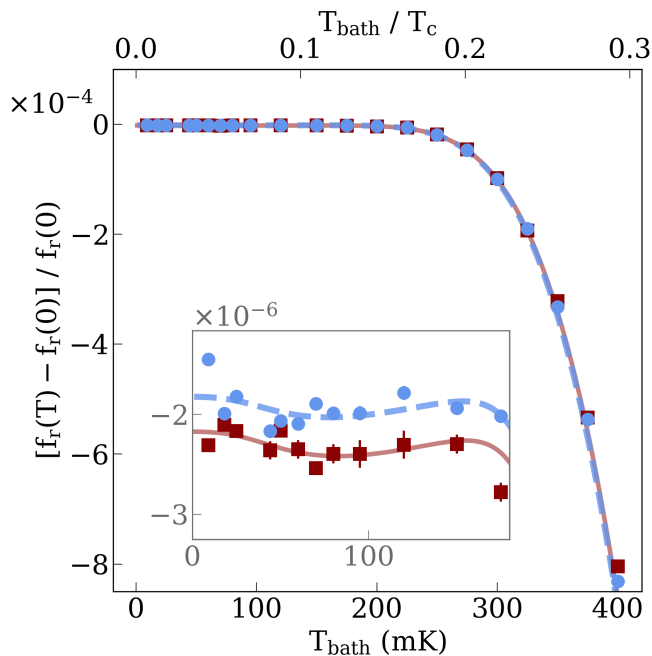


FIG. 4. The relative shift in resonant frequency as a function of device temperature (at a fixed low  $P_{\text{read}}$ ). The red data and fit are for the  $\lambda/2$  resonator and the blue data and fit are for the  $\lambda/4$  resonator. The cutout gives a closer look at the fit in the 0 to 175 mK regime, where TLS effects strongly dominate.

loss. The TLS-dependent change in resonant frequency,  $\delta f_{\text{TLS}}$ , can be modeled as [5, 16]

$$\begin{aligned} \delta f_{\text{TLS}}(T_{\text{bath}}) &= \frac{f_r(T_{\text{bath}}) - f_r(0)}{f_r(0)} \\ &= F \delta_{\text{TLS}}^0 \times \left( \text{Re} \left[ \psi \left( \frac{1}{2} + \frac{\xi}{i} \right) \right] - \ln(2\xi) \right) \end{aligned} \quad (14)$$

where  $\psi$  is the Digamma function.

At high temperatures ( $\geq 200$  mK)  $\delta f_{\text{th}}$  should very strongly dominate the total temperature-dependent frequency shift, allowing us to fit our  $df_r/dT_{\text{bath}}$  data to Eq. 13 (for a fixed intermediate power). Using this method we recover  $\alpha = 0.25$  and  $T_c = 1.37$ . We are then able to use this  $\alpha$  and  $T_c$  with equations 12, 13, and 14 to recover  $F\delta_{\text{TLS}}^0$  and  $f_r(0)$  by fitting our low-temperature  $df_r/dT_{\text{bath}}$  data (for a fixed low power). Using this method we recover for the  $\lambda/2$  and  $\lambda/4$  respectively, and  $F\delta_{\text{TLS}}^0$  ( $\times 10^{-6}$ ) = [3.71, 3.10] (tables II, III).

#### IV. RESULTS AND DISCUSSION

All data fits were performed using bootstrapped least-squares fitting. We find that  $Q_c$  is generally invariant across measurement conditions ( $Q_c[\lambda/2, \lambda/4] = [0.87, 2.58] \times 10^5$ ) as expected excepting measurements

at the highest read tone powers, where the resonator response bifurcates and our model ceases to apply (these data are therefore excluded). We measured minimum  $Q_i^{-1}$  ( $\times 10^{-8}$ ) values of 3.64, and 8.57 for the half-wave and the quarter-wave resonators respectively.

Generally the total loss in bulk superconducting aluminum is around  $\delta$  ( $\times 10^{-4}$ )  $\approx 2 - 30$  [11]. However, for thin film Al resonators, both the total loss and its relative contributions vary significantly with resonator design and fabrication methods. Generally for thin film resonators groups have measured  $F\delta_{\text{TLS}}^0$  ranging between a few  $\times 10^{-7}$  [17, 18] and  $1 \times 10^{-5}$  [19], with typical values falling within the few  $\times 10^{-6}$  range [11]. It is not clear how much this variance in  $F\delta_{\text{TLS}}^0$  can be truly attributed to different TLS populations, as opposed to the impacts of different geometries (different  $F$  values), and differences in the models used to extract  $F\delta_{\text{TLS}}^0$  from measurement data. For our device we approximate  $F \sim 8.1 \times 10^{-3}$  (by rescaling the calculations in [5] for  $\text{Al}_2\text{O}_3$  and our resonator geometry). Using this  $F$  we expect a  $\delta_{\text{TLS}}^0 \approx 3 - 5 \times 10^{-4}$  for our thin film Al. In comparison, studies of 480 nm thick  $\text{AlO}_x$  resonators have found  $\delta_{\text{TLS}}^0 \approx 1.3 \times 10^{-3}$  [20].

TABLE II. Film parameter results from fits to measurements for the  $\lambda/2$  resonator. Column two contains the fit results for the composite  $dQ_i^{-1}/dP_{\text{read}}$  data across all temperatures. Columns one and three contain fit results from the low probe tone power regime.

	$dQ_i^{-1}/dT$	$dQ_i^{-1}/dn_{\text{ph}}$	$\delta f_r/f_r(T=0)$
$\alpha$	$0.255 \pm 0.006$	–	$0.251 \pm 0.003$
$T_c$ (K)	$1.367 \pm 0.003$	–	$1.369 \pm 0.004$
$F\delta_{\text{TLS}}^0$ ( $\times 10^{-6}$ )	$3.87 \pm 0.21$	$3.85 \pm 0.23$	$3.71 \pm 0.89$
$n_{\text{ph}}^c$	$386 \pm 43$	$364 \pm 54$	–
$\mu$	$1.32 \pm 0.17$	–	–
$\beta$	–	$0.76 \pm 0.05$	–
$\eta_{\text{read}}$ ( $\times 10^{-3}$ )	–	$1.7 \pm 0.4$	–
$Q_{\text{other}}^{-1}$ ( $\times 10^{-8}$ )	–	$3.83 \pm 1.3$	–

TABLE III. Film parameter results from fits to measurements for the  $\lambda/4$  resonator. Column two contains the fit results for the composite  $dQ_i^{-1}/dP_{\text{read}}$  data across all temperatures. Columns one and three contain fit results from the low probe tone power regime.

	$dQ_i^{-1}/dT$	$dQ_i^{-1}/dn_{\text{ph}}$	$\delta f_r/f_r(T=0)$
$\alpha$	$0.259 \pm 0.01$	–	$0.251 \pm 0.003$
$T_c$	$1.366 \pm 0.007$ K	–	$1.365 \pm 0.004$
$F\delta_{\text{TLS}}^0$ ( $\times 10^{-6}$ )	$3.47 \pm 0.08$	$3.29 \pm 0.40$	$3.10 \pm 0.79$
$n_{\text{ph}}^c$	$492 \pm 91$	$441 \pm 76$	–
$\mu$	$1.23 \pm 0.05$	–	–
$\beta$	–	$0.78 \pm 0.04$	–
$\eta_{\text{read}}$ ( $\times 10^{-3}$ )	–	$1.8 \pm 0.5$	–
$Q_{\text{other}}^{-1}$ ( $\times 10^{-8}$ )	–	$7.23 \pm 0.7$	–



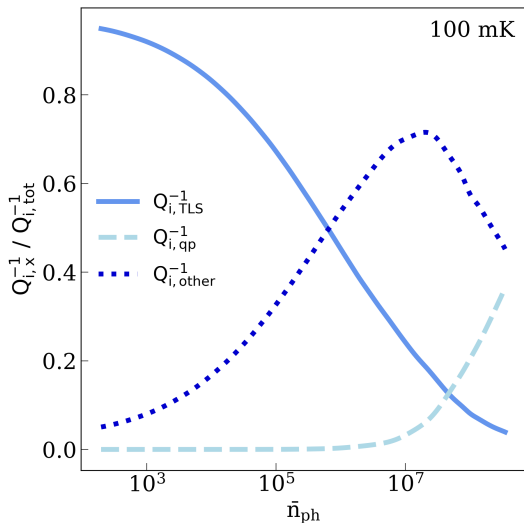


FIG. 5. Fractional contributions to the total loss as a function of average photon occupation number in the resonator  $\bar{n}_{ph}$ . This example is for the  $\lambda/4$  resonator at 100 mK. The lines were made using the model from Section III and interpolating between the data. For this temperature, at high  $\bar{n}_{ph}$  the device enters a regime where the total loss is dominated by the inherent (non power or temperature dependent) resonator loss  $Q_{i,other}^{-1}$ .

We also observed that at the lowest temperatures and photon occupation numbers, our loss data deviated significantly from the standard TLS model, in part motivating the model we present in Section III. We observed that our data generally deviated from the standard TLS model around 60 mK or  $hf_r/k_b T \sim 3$ . At these very low temperatures and photon occupation numbers, the standard model predicts total loss increasing before leveling off. In our data we observe the total loss continuing to decrease as the temperature and power approach zero.

Some works have suggested that this anomalous loss behavior is the product of TLS response bandwidths decreasing with decreasing temperatures, eventually locking out TLS with relatively long fluctuation timescales [21]. We explored using this method to model the TLS behavior in our data, but achieved better fitting (with fewer free-parameters) with the model presented in Section III. We were able to fit this regime by first assum-

ing that the average photon occupation number has some power and temperature dependence, and by replacing the critical photon number  $n_{ph}^c$  from the standard model with a temperature-dependent term (Eq. 11).

Interestingly, at low enough temperatures (below 200 mK) we observed ranges of intermediate-high photon occupation numbers where  $Q_{i,other}^{-1}$  becomes the dominant source of loss (Figure 5). We found that at low temperatures this regime spans a wide range of powers, but narrows significantly as temperature increases, and disappears completely somewhere between 150 and 200 mK and for all warmer temperatures (as  $Q_{i,qp}^{-1}$  overtakes the other loss contributions). This suggests that at their intended operation temperature of 100 mK, our resonators are not dominated by TLS or quasiparticle loss when read-out at high enough powers. In this regime, TLS and quasiparticle loss each contribute between 2-15% of the total loss. We believe that our wide architecture (width/gap 10/5) may be responsible for creating this  $Q_{i,other}^{-1}$  dominated regime by allowing us to accommodate higher photon occupation numbers before bifurcation occurs. As a result we are able to suppress TLS loss to a greater degree.

## V. CONCLUSION

In conclusion, we found that our device has an average-to-good  $F\delta_{TLS}^0 \sim$  a few  $\times 10^{-6}$  compared to similar thin film Al devices. Despite our average  $F\delta_{TLS}^0$ , we observed a higher than expected level of TLS loss suppression in our devices at high photon occupation numbers. We observed a regime between low and high powers where our inherent device loss  $Q_{i,other}^{-1}$  was dominant over TLS and quasiparticle loss. In this regime we found our minimum loss to be  $Q_{i,other}^{-1} \sim$  a few  $\times 10^{-8}$ . We posit that our broad width/gap ratio may be responsible for this effect, by allowing us to drive our devices to higher powers.

At very low temperatures and photon occupation numbers we observed that the standard TLS loss model deviated from our data, and instead we were able to successfully model this regime by adding parameters to account for changes in the TLS population's average relaxation time  $T_1$  and average dephasing time  $T_2$ , and accounting for the fact that different photon occupation modes will saturate the TLS systems differently (via  $\bar{n}_{ph}^\beta$ ).

- 
- [1] M. S. Khalil, M. Stoutimore, F. Wellstood, and K. Osborn, An analysis method for asymmetric resonator transmission applied to superconducting devices, *Journal of Applied Physics* **111** (2012).
  - [2] J. Gao, *The physics of superconducting microwave resonators* (California Institute of Technology, 2008).
  - [3] S. Probst, F. Song, P. A. Bushev, A. V. Ustinov, and M. Weides, Efficient and robust analysis of complex scattering data under noise in microwave resonators, *Review*

of Scientific Instruments **86** (2015).

- [4] F. W. Carter, T. S. Khaire, V. Novosad, and C. L. Chang, scraps: An open-source python-based analysis package for analyzing and plotting superconducting resonator data, *IEEE Transactions on Applied Superconductivity* **27**, 1 (2016).
- [5] J. Gao, M. Daal, A. Vayonakis, S. Kumar, J. Zmuidzinas, B. Sadoulet, B. A. Mazin, P. K. Day, and H. G. Leduc, Experimental evidence for a surface distribution of two-

- level systems in superconducting lithographed microwave resonators, *Applied Physics Letters* **92** (2008).
- [6] J. Zmuidzinas, Superconducting microresonators: Physics and applications, *Annu. Rev. Condens. Matter Phys.* **3**, 169 (2012).
- [7] D. Goldie and S. Withington, Non-equilibrium superconductivity in quantum-sensing superconducting resonators, *Superconductor Science and Technology* **26**, 015004 (2012).
- [8] D. Flanigan, *Kinetic inductance detectors for measuring the polarization of the cosmic microwave background* (Columbia University, 2018).
- [9] O. Noroozian, *Superconducting microwave resonator arrays for submillimeter/far-infrared imaging* (California Institute of Technology, 2012).
- [10] S. B. Kaplan, C. Chi, D. Langenberg, J.-J. Chang, S. Jafarey, and D. Scalapino, Quasiparticle and phonon lifetimes in superconductors, *Physical Review B* **14**, 4854 (1976).
- [11] C. R. H. McRae, H. Wang, J. Gao, M. R. Vissers, T. Brecht, A. Dunsworth, D. P. Pappas, and J. Mutus, Materials loss measurements using superconducting microwave resonators, *Review of Scientific Instruments* **91** (2020).
- [12] W. A. Phillips, Two-level states in glasses, *Reports on Progress in Physics* **50**, 1657 (1987).
- [13] K. D. Crowley, R. A. McLellan, A. Dutta, N. Shumiya, A. P. Place, X. H. Le, Y. Gang, T. Madhavan, M. P. Bland, R. Chang, *et al.*, Disentangling losses in tantalum superconducting circuits, *Physical Review X* **13**, 041005 (2023).
- [14] J. Burnett, L. Faoro, I. Wisby, V. L. Gurtovoi, A. V. Chernykh, G. M. Mikhailov, V. A. Tulin, R. Shaikhaidarov, V. Antonov, P. J. Meeson, *et al.*, Evidence for interacting two-level systems from the  $1/f$  noise of a superconducting resonator, *Nature Communications* **5**, 4119 (2014).
- [15] L. Faoro and L. B. Ioffe, Interacting tunneling model for two-level systems in amorphous materials and its predictions for their dephasing and noise in superconducting microresonators, *Physical Review B* **91**, 014201 (2015).
- [16] S. Kumar, J. Gao, J. Zmuidzinas, B. A. Mazin, H. G. LeDuc, and P. K. Day, Temperature dependence of the frequency and noise of superconducting coplanar waveguide resonators, *Applied Physics Letters* **92** (2008).
- [17] L. Chayanun, J. Biznárová, L. Zeng, P. Malmberg, A. Nylander, A. Osman, M. Rommel, P. L. Tam, E. Olsson, P. Delsing, *et al.*, Characterization of process-related interfacial dielectric loss in aluminum-on-silicon by resonator microwave measurements, materials analysis, and imaging, *APL Quantum* **1** (2024).
- [18] C. J. Richardson, N. P. Siwak, J. Hackley, Z. K. Keane, J. E. Robinson, B. Arey, I. Arslan, and B. S. Palmer, Fabrication artifacts and parallel loss channels in metamorphic epitaxial aluminum superconducting resonators, *Superconductor Science and Technology* **29**, 064003 (2016).
- [19] A. D. O'Connell, M. Ansmann, R. C. Bialczak, M. Hofheinz, N. Katz, E. Lucero, C. McKenney, M. Neeley, H. Wang, E. M. Weig, *et al.*, Microwave dielectric loss at single photon energies and millikelvin temperatures, *Applied Physics Letters* **92** (2008).
- [20] D. P. Pappas, M. R. Vissers, D. S. Wisbey, J. S. Kline, and J. Gao, Two level system loss in superconducting microwave resonators, *IEEE Transactions on Applied Superconductivity* **21**, 871 (2011).
- [21] T. Tai, J. Cai, and S. M. Anlage, Anomalous loss reduction below two-level system saturation in aluminum superconducting resonators, *Advanced Quantum Technologies* **7**, 2200145 (2024).